

Knockdown of AT-rich interaction domain (ARID) 5B gene expression induced AMPK α 2 activation in cardiac myocytes

Lisa Hirose-Yotsuya^{1,*}, Fumio Okamoto^{1,2}, Takahiro Yamakawa¹, Robert H. Whitson¹, Yoko Fujita-Yamaguchi^{1,3}, Keiichi Itakura¹

¹Department of Molecular & Cellular Biology, Beckman Research Institute of City of Hope, Duarte, California, USA;

²Emergency Medicine and Cardiology of Takatsuki Red Cross Hospital, Osaka, Japan;

³Department of Diabetes Complications & Metabolism, Beckman Research Institute of City of Hope, Duarte, California, USA.

Summary

This study demonstrated that ARID5B mRNA is present in mouse cardiomyocyte HL-1 cells, and that ARID5B siRNA constantly knocked down ARID5B gene expression to the 40% level of control. AMPK α 2 protein was elevated in such ARID5B knockdown HL-1 cells, and this was accompanied by an increase in the level of phosphorylated AMPK α . Since AMPK α 2 mRNA levels did not change in ARID5B knockdown cells, the stability of AMPK α 2 protein was investigated using inhibitors for protein synthesis and proteasomal degradation. Treatment of HL-1 cells with either cycloheximide or MG132 caused an appreciable increase in the amount of AMPK α 2 protein in ARID5B knockdown cells, which suggests that knockdown of ARID5B mRNA extends the half-life of AMPK α 2 protein in HL-1 cells *via* yet unidentified mechanisms. As for the expected downstream consequences of AMPK α 2 activation, we found thus far that glucose uptake, fatty acid uptake, or fatty acid oxidation remained unchanged in HL-1 cells after knockdown of ARID5B. Further studies are required to understand the mechanisms for ARID5B knockdown and resulting AMPK α 2 activation, and also to identify which metabolic pathways are affected by AMPK α 2 activation in these cells. In summary, this study provided the foundation for an *in vitro* cell culture system to study possible roles of ARID5B in cardiomyocytes.

Keywords: Mrf-2, ARID5B, downregulation by siRNA, AMPK α 2 activation, cardiac myocytes, HL-1 cells

1. Introduction

ARID5B (AT-rich interaction domain-containing protein 5B) was previously known as Mrf-2 (modulator recognition factor 2). It was identified in our laboratory in 1996 as a novel nuclear protein that binds to sequences upstream of the human cytomegalovirus major immediate-early enhancer/promoter and exerts repressor activity in undifferentiated human Tera-2 cells (1). Subsequent studies revealed the three-dimensional structure of the novel DNA-binding motif (ARID) of Mrf-2 and mechanisms of DNA recognition (2-4). The

ARID family of DNA-binding proteins has grown since then to include fifteen proteins found in humans and most other vertebrate species, and six proteins found in *Drosophila* as well as proteins found in worms, fungi, plants and yeast (5-8). The ARID family is divided into six sub-families. In addition to a variety of roles as transcription factors in cell growth, differentiation, and development (6), a number of studies have suggested that proteins in most of the ARID sub-families are involved in cancer as tumor suppressors or promoters (8). A notable exception is the ARID5 sub-family which consists of two members, Mrf-1/ARID5A and Mrf-2/ARID5B (7,8). Mrf-2/ARID5B is expressed in various tissues including mouse cardiac and vascular tissues, where it seems to regulate smooth muscle cell differentiation and proliferation (9), lung, kidney, and brain as well as less abundantly in adrenal gland, spleen and thymus (10). Important roles of ARID5B in growth, immune, and sexual development have been

*Address correspondence to:

Dr. Lisa Hirose-Yotsuya, Department of Molecular Metabolic Regulation, Diabetes Research Center, Research Institute National Center for Global Health and Medicine, 1-21-1 Toyama, Shinjuku-ku, Tokyo 162-8655, Japan (current address). E-mail: ryotsuya@ri.ncgm.go.jp

suggested (10). While the role of ARID5B in cancer is still elusive, previous studies suggested that genetic variations in the *ARID5B* gene are associated with susceptibility to coronary atherosclerosis or type 2 diabetes in Japanese populations (11,12).

Targeted disruption of the *ARID5B* gene resulted in slower neonatal weight gains, high rates of mortality in neonates, and significant reductions in adult weight and adiposity (13). This suggested that *ARID5B* is essential for embryonic development and accumulation of lipids in postnatal life. Studies using mouse embryonic fibroblasts (MEFs) derived from *ARID5B*^{-/-} embryos and *ARID5B*^{+/+} littermate controls demonstrated that adipogenesis in *ARID5B*^{-/-} MEFs was significantly lower than that in *ARID5B*^{+/+} MEFs, but was restored when *ARID5B* was expressed in *ARID5B*^{-/-} MEFs (14). Similarly, the expression of multiple adipogenic genes was inhibited following transient transfection of siRNA targeting *ARID5B* in 3T3-L1 cells (14). Since a role of *ARID5B* in the regulation of metabolism has been suggested (11-13), we investigated the potential involvement of *ARID5B* and AMP-activated protein kinase (AMPK) in the metabolism of cardiac myocytes.

AMPK has been known as a sensor and regulator of energy balance at the cellular level as well as at the whole body level by responding to hormonal and nutrient signals (15-17). Multiple AMPK subunit isoforms encoded by distinct genes were identified with two α subunits ($\alpha 1$ and $\alpha 2$), two β subunits ($\beta 1$ and $\beta 2$), and three γ subunits ($\gamma 1$, $\gamma 2$, and $\gamma 3$) (15,16). The α subunit is a kinase which is activated by phosphorylation in response to an increase in the AMP:ATP ratio. Binding of AMP to the γ subunit of the AMPK $\alpha\beta\gamma$ complex induces conformational changes in the α subunit kinase leading to the critical Thr172 phosphorylation by its upstream kinases. Although the mechanisms of these signaling pathways are not fully understood, it has been well-documented that activation of AMPK in skeletal and cardiac muscles is induced by metabolic stress and whole-body energy status as well as the AMPK mimetic AICAR and diabetic drugs such as metformin (15,18,19).

Previous studies showed that AICAR increased glucose uptake in heart muscle, indicating that AMPK may be involved in GLUT4 translocation (20), and that AMPK and PI-3K/Akt had an additive effect on oxidative stress-mediated GLUT4 translocation in cardiac myocytes (21). Furthermore, mice lacking AMPK $\alpha 2$ or expressing dominant negative AMPK $\alpha 2$ inhibited the ischemia-induced stimulation of glucose uptake in cardiac myocytes (22-24). These studies strongly suggested that AMPK $\alpha 2$ plays an important role in regulating cardiac glucose metabolism and protecting the heart from metabolic stresses.

The current study tested the hypothesis that *ARID5B* plays a role in glucose metabolism *via* the AMPK signaling pathway in cardiac myocytes. We found that

when siRNA was introduced to HL-1 cardiomyocytes, *ARID5B* mRNA was significantly reduced, and that the levels of both total and phosphorylated AMPK $\alpha 2$ subunit were significantly increased. The mechanism and functional consequences of the AMPK $\alpha 2$ activation induced by *ARID5B* knockdown in HL-1 cells were also investigated. Although not conclusive, this study provided a good model system for further studying the role of *ARID5B* knockdown in AMPK $\alpha 2$ signaling pathways.

2. Materials and Methods

2.1. Materials

Mouse HL-1 cardiomyocytes were provided by Dr. W. Claycomb (Louisiana State University Health Science Center, New Orleans, LA) (25,26). Claycomb medium, fetal bovine serum (FBS), penicillin-streptomycin, norepinephrine, L-glutamine, trypsin-EDTA, trypsin inhibitor, fibronectin, cytochalasin B, cycloheximide, and MG132 were purchased from Sigma-Aldrich. L-Ascorbic acid sodium salt was from Mallinckrodt. Opti-MEM and Lipofectamine[®] RNAiMAX Transfection Reagent were from Life technologies. Bacto gelatin, ON-TARGETplus Mouse *ARID5B* siRNA-SMART pool (siRNA), ON-TARGETplus Non-targeting Pool (control scramble RNA), Tris-HEPES gels, and 20 \times Tris-HEPES buffer for sodium dodecyl sulfate polyacrylamide gel electrophoresis (SDS-PAGE) were obtained from Thermo Fisher Scientific. Polyvinylidene difluoride (PVDF) membrane was from GE Healthcare Life Sciences. 10 \times TBS was from Bio-Rad. Non-fat milk was from Labscientific, Inc. HyGLO Chemiluminescent HRP Antibody Detection Reagent was from Denville Scientific Inc. 2-Deoxy-D-[³H] glucose and [³H]palmitic acid were from American Radiolabel Chemicals.

2.2. Cell culture

HL-1 cells were grown as monolayer cultures in flasks, dishes, and plates precoated with 2 $\mu\text{g}/\text{cm}^2$ fibronectin dissolved in 0.02% gelatin. HL-1 cells were maintained in Claycomb medium supplemented with 10% FBS, 2 mM L-glutamine, 0.1 mM norepinephrine (prepared freshly from 10 mM stock solution in 30 mM L-ascorbic acid), and 100 $\mu\text{g}/\text{mL}$ penicillin-streptomycin. Cells were grown at 37°C in an atmosphere of 5% CO₂. The medium was changed every other day.

2.3. siRNA transfection

The transfection procedure is summarized in Figure 1. We used a commercially-available mixture of four double-stranded siRNAs with the following sequences on the sense strand; 5'-acaauaacugugacgguaa-3',

5'-gugaugaguucgcccga-3', 5'-cggagaagaucacagca-3', and 5'-gguccaugcuuaacggau-3'. These siRNA's target exons 5, 4-plus- 5, 10, and 4, respectively of *ARID5B*. Cells were seeded in 24-well plates, 12-well plates, or 35 mm dishes (2.5×10^4 cells/cm²), and transfected 24 h after seeding. At that time (40-50% confluence), the cells were incubated for 2-3 h in Claycomb medium without penicillin and streptomycin, then transfected with 50 nM siRNA or control scramble RNA using Lipofectamine[®] RNAiMAX Transfection Reagent. After 24 h, the medium was replaced by Claycomb medium without penicillin and streptomycin. Cells were used for molecular and cellular experiments at 48 h post-transfection. To confirm the effect of siRNA, cells were lysed with 700 μ L of Qiazol (Qiagen), and RNA was isolated with Qiagen RNeasy[®]. *ARID5B* mRNA level was determined by quantitative real-time PCR as described in section 2.4.

2.4. Quantitative real-time PCR

Total RNA samples (1 μ g) were reverse-transcribed with High-Capacity cDNA Reverse Transcription Kit (Life technologies), and the resulting cDNA samples were amplified with the specific primer pairs for mouse *ARID5B* and *Rpl19* as a control housekeeping gene using iQ SYBR Green Super Mix (Bio-Rad). The sequences of specific primer pairs used were as follows. *ARID5B* forward, 5'-agaaaacgccatcgagc-3'; reverse, 5'-ctcccaggattaccactaac-3' and *Rpl19* forward, 5'-agcctgtgactgtccattcc-3'; reverse, 5'-gcagtaccctctcttcc-3'. The reaction was performed using the following temperature cycles, initial denaturation at 95°C for 10 min followed by 40 cycles of amplification at 95°C for 10 sec and 56°C for 30 sec (*ARID5B*), or 40 cycles of amplification at 95°C for 10 sec and 61°C for 30 sec (*Rpl19*). The mRNA expression level was determined using the CFX96 real-time detection system (Bio-Rad). Relative gene expression was calculated using the $\Delta\Delta$ CT method.

2.5. Western blotting analysis

At 48 h post-transfection, cells were washed twice with ice-cold PBS and lysed using ice-cold cell lysis buffer (50 mM HEPES, pH 7.4, containing 2 mM Na₃VO₄, 10 mM Na₄P₂O₇, 10 mM NaF, 2 mM EDTA 2Na, 2 mM EGTA, and 0.2 mM PMSF). After incubation on a shaker for 15 min at 4°C, cell lysates were centrifuged at 14,000 rpm at 4°C for 15 min. Protein concentrations in the cleared lysates were measured by BCA assay (Thermo Fisher Scientific). Samples of 10-20 μ g were subjected to SDS-PAGE using Tris-HEPES gels and then transferred to PVDF membranes. The membranes were blocked with 5% non-fat milk in TBST buffer (TBS containing 0.1% Tween 20) for 1 h at room temperature. After blocking, membranes were

incubated at 4°C overnight with the following primary antibodies; anti-phospho-AMPK α (1:1000, #2535) and anti-AMPK α (1:1000, #2603) from Cell Signaling Technology, anti-AMPK α 2 (1:1000, ab97275) from Abcam, anti-EFTUD2 (1:2000, 10208-1-AP) from Proteintech, and anti-GAPDH (1:10000, AM4300) from Ambion. Subsequently, the membranes were washed 3 times with TBST for 5 min and incubated with HRP-conjugated anti-rabbit IgG (#170-6515, Bio-Rad) or HRP-conjugated anti-mouse IgG (sc-2005, Santa Cruz) for 1 h at room temperature. Then, the membranes were washed 4 times with TBS containing 0.1% Tween 20 and 0.1% Triton X-100 for 5 min at room temperature, then incubated with HyGLO Chemiluminescent HRP Antibody Detection Reagent. The membranes were exposed to X-ray film, and the protein bands on the films were quantified using Image J software.

2.6. Analysis of AMPK α 2 protein stability

HL-1 cells in 35 mm dishes were transfected with siRNA as described in 2.3, and at 48 h post-transfection, the growth medium was changed to medium containing 5 μ g/mL cycloheximide (CHX) or 10 μ M MG132, a proteasomal degradation inhibitor. Cells were harvested at different time points after CHX or MG132 treatment, and AMPK α 2 and GAPDH protein levels were determined by Western blotting.

2.7. Glucose and fatty acid uptake assays in HL-1 cells

Cells were grown in 24-well plates and transfected with siRNA as described in section 2.3. Cells were washed with KRPH buffer (130 mM NaCl, 4.7 mM KCl, 1.24 mM MgSO₄, 2.5 mM CaCl₂, 1 mM HEPES, 2.5 mM NaH₂PO₄) once at 48 h post-transfection. Then cells were incubated in 250 μ L of fresh KRPH buffer for 15 min at 37°C. For the glucose uptake assay, HL-1 cells were incubated with [³H]2-deoxy-D-glucose (10 μ M; 137.5 μ Ci/well) for 10 min at 37°C. The incubation medium was aspirated, then the cells were washed four times with ice-cold PBS and solubilized by adding 100 μ L of 0.5 M NaOH to each well. Aliquots of the cell extracts were transferred to vials for scintillation counting. In order to determine the level of non-specific background, cells in replicate wells were pre-treated with 20 μ M cytochalasin B for 15 min at 37°C, incubated with [³H]2-deoxy-D-glucose, and processed in the same way. Aliquots of the same cell extracts were used for determining protein concentrations by BCA assay. Results were calculated as pmol of glucose uptake per min per mg of protein.

For fatty acid uptake assays, cells were incubated for 15 min at 37°C in KRPH buffer, and [³H] palmitic acid (40 μ M; 10.5 μ Ci/well) was added to each well. After a 20 min-incubation at 37°C, the medium was removed, the cells were washed 4 times with ice-cold

PBS, and solubilized with 100 μ L of 0.5 M NaOH per well. The radioactivity in both the incubation medium and the cell lysate from each well were measured by scintillation counting. The percentage of fatty acid uptake was calculated by dividing ^3H in the cell lysate by total ^3H from both the cell lysate and incubation medium.

2.8. Positron Emission Tomography (PET) for glucose uptake in the heart of *ARID5B* knockout mice

Animal studies were approved by the City of Hope Animal Care and IACUC. Generation of the total body *ARID5B* knockout mice has been previously described (13). Mice were housed in a temperature-controlled environment with a 12 h light: 12 h dark cycle and allowed *ad libitum* access to standard chow and water.

Thirty two week-old male mice were used for these experiments. The ^{18}F -fluorodeoxyglucose (^{18}F -FDG) radio-tracer was obtained from the City of Hope radiopharmacy. The mice were imaged at the City of Hope Small Animal Imaging Core on two days: On the first day, two *ARID5B*^{-/-} males and one *ARID5B*^{+/+} male littermate control were imaged; on the second day, one *ARID5B*^{-/-} male and two *ARID5B*^{+/+} male littermate controls were imaged. The average weight for the *ARID5B*^{-/-} males was 25.7 ± 4.0 grams; the average weight for the *ARID5B*^{+/+} males was 41.3 ± 4.1 grams ($p < 0.05$). Prior to imaging, the mice were placed in individual cages with Sani-chip bedding, and fasted overnight (from 5:30 PM to 9:00 AM). The mice were placed in a cage with a warming light for 15 min prior to injection *via* the tail vein with 121-177 μCi of ^{18}F -FDG, and then moved to cages without warming lights for uptake periods of 58-60 min. Following the uptake period, tail regions of the mice were imaged for 2 min to insure that there was no extravasation

of the tracer from the injection site. The mice were imaged for 10 min while under isoflurane anesthesia. Following the imaging scans, the mice were euthanized under isoflurane, and various organs and tissues were harvested. The tissue samples were weighed, and the ^{18}F in each sample was measured using a gamma counter. The CPM values were corrected for the radioactive decay that occurred in the interval following the injection. Imaging data were analyzed using the ASI-Pro software package. Specific uptake values in the heart were estimated as follows. The PET images were rotated so that a series of transverse optical sections of the heart could be analyzed. In each optical section both the heart plus the enclosed blood space and the blood space alone were analyzed by defining the appropriate regions of interest. The volume of heart tissue was calculated as the volume of heart-plus-blood minus the volume of blood alone. Similarly, the total DPM of ^{18}F per cc in the heart was as calculated by subtracting the blood space values from the heart-plus-blood space values. Specific uptake values are expressed as (DPM/cc tissue)/(injected dose in $\mu\text{Ci}/\text{ml}$ blood). The blood volume was calculated as 5.85% of total body weight.

2.9. Statistics

Data are expressed as mean \pm SEM. Differences were evaluated by two-tailed Student *t* test. Statistical significance was set at $p < 0.05$.

3. Results

3.1. *ARID5B* gene expression was reduced in HL-1 cardiomyocytes by siRNA

The siRNA transfection protocol as schematically illustrated in Figure 1 was used throughout this study.

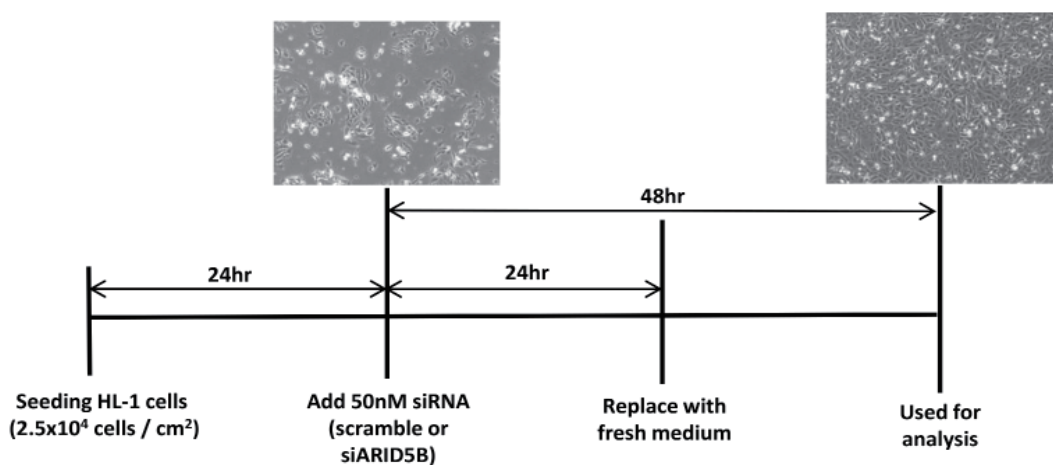


Figure 1. Schematic diagram of the siRNA transfection protocol used in this study. HL-1 cardiomyocytes were seeded in 24-well plates, 12-well plates, or 35 mm dishes with a density of 2.5×10^4 cells/cm². Cells were cultured for 24 h to reach 40-50% confluence (inset, left panel) before transfection of siRNA or control scramble RNA as described in Methods. At 24 h post-transfection (inset, right panel), the medium was replaced with fresh medium to allow HL-1 cells to recover. At 48 h post-transfection, cells were subjected to various analyses.

HL-1 cardiomyocytes were cultured for 24 h to allow them to attach to the plates (Figure 1 insets, left panel) before being treated with siRNA or scramble RNA for 24 h. The transfection medium was replaced with fresh culture medium and the resulting HL-1 cardiomyocytes were subjected to cellular and molecular analyses at 48 h post-transfection (Figure 1 insets, right panel).

In each experiment, the level of ARID5B expression in HL-1 cells was determined by quantitative real-time PCR. The results of nine independent experiments showed that the mRNA level in cells treated with ARID5B siRNA was always ~38% of the value for cells treated with control scramble RNA (Mean \pm SE: 37.7 ± 2.1 %, $n = 9$, $p < 0.001$). Results of representative experiments are shown in Figures 2A, 3A, 4A, and 5A. This indicates not only that ARID5B mRNA is present in HL-1 cells, but also that siRNA efficiently knocked down gene expression.

3.2. Both AMPK α 2 protein and AMPK α phosphorylation levels were elevated by knockdown of ARID5B mRNA

After confirming siRNA downregulated ARID5B

mRNA (Figure 2A), we determined AMPK α protein levels by Western blotting. As seen in Figure 2B, Western blotting analysis of cell lysates with anti-AMPK α 1 or anti-AMPK α 2 antibody clearly showed that the AMPK α 2 protein level was significantly increased in cells transfected with ARID5B siRNA, but that no change was observed in the AMPK α 1 protein level (Figure 2B). Quantitation of immunostained bands from four experiments revealed an average increase of 1.4-fold (1.4 ± 0.15 , $n = 4$, $p < 0.05$) in AMPK α 2 protein level (Figure 2C, right panel) but no change in the AMPK α 1 protein level (Figure 2C, left panel).

The phosphorylation status of T172 of AMPK α was also determined by Western blotting using anti-phospho AMPK α . This monoclonal antibody was produced by immunizing animals with a synthetic phospho-peptide corresponding to amino acid residues surrounding Thr172 of human AMPK α protein. Because this amino acid sequence is conserved between mouse and humans and between AMPK α 1 and AMPK α 2 in both species, the antibody recognizes phospho-Thr172 in both AMPK α 1 and AMPK α 2. Thus, in order to assess AMPK α phosphorylation, the levels of total AMPK α protein (AMPK α 1 plus α 2)

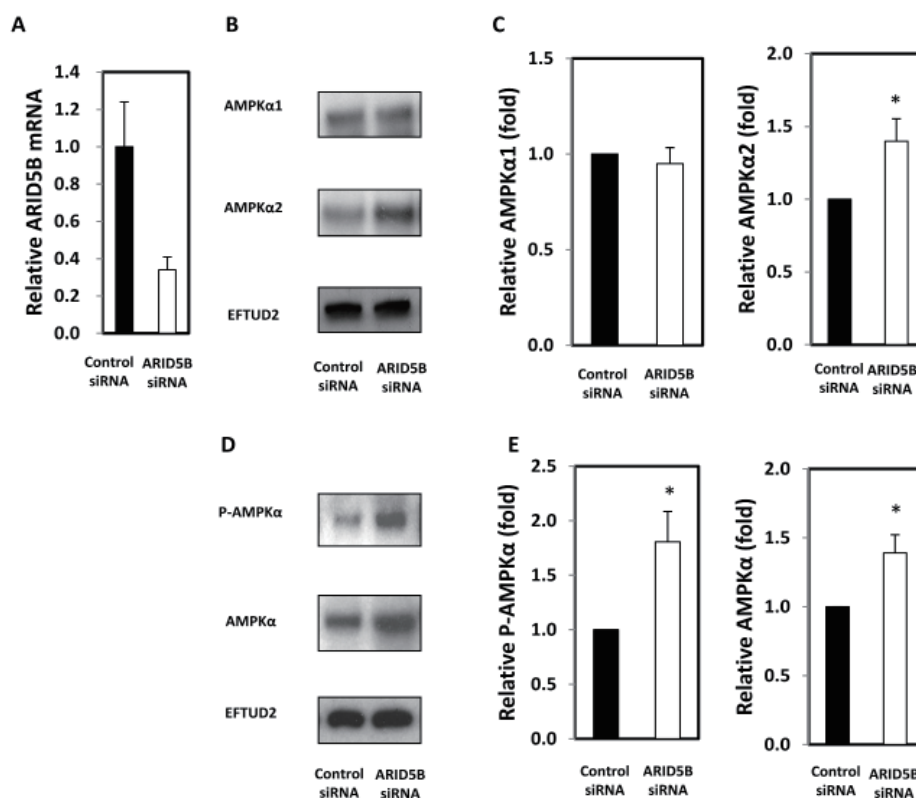


Figure 2. AMPK protein expression levels in control and ARID5B knockdown HL-1 cells. **A:** HL-1 cells were seeded in 12-well plates. siRNA efficiency was confirmed by qPCR at 48 h post-transfection. **B:** The levels of AMPK α 1 and α 2 proteins were examined by Western blotting with subunit-specific antibodies. Cell lysates (10–20 μ g of protein per lane) were subjected to SDS-PAGE and immunoblotted as described in Methods. EFTUD2 was used as a loading control. A representative Western blotting result of four independent experiments is shown. **C:** Quantitation of AMPK α 1 or α 2 bands ($n = 4$; $*p < 0.05$). **D:** Total AMPK α protein and total AMPK α phospho-protein levels were examined by Western blotting. Cell lysates (10 μ g protein per lane) were subjected to SDS-PAGE and blotted with primary antibodies as described in Methods. EFTUD2 was used as a loading control. A representative result of four independent experiments is shown. **E:** Quantitation of AMPK α or phospho-AMPK α bands as shown in **D** ($n = 4$; $*p < 0.05$). In **A**, **C**, and **E**, shown are results from control (■) and ARID5B siRNA experiments (□).

and the combined levels of phosphorylated AMPK α 1 plus α 2 were measured by Western blotting. Figure 2D clearly shows an increase in the amount of total AMPK α protein. Since the experiments shown in Figures 2B and 2C indicate that AMPK α 2 increases while AMPK α 1 does not, it is clear that the increase in total AMPK α protein is due solely to the increase in AMPK α 2. Figure 2E (right panel) revealed the increase in total AMPK α (1.4 ± 0.13 -fold, $n = 4$, $p < 0.05$), which is consistent with the increase in AMPK α 2 shown in Figure 2C (right panel). Figure 2D and E clearly show that the increase in total phospho-AMPK α (1.8 ± 0.28 -fold, $n = 4$, $p < 0.05$) is also significant and even greater than the increase in total AMPK α . Although other possibilities must be considered, these results, taken together, strongly suggest that ARID5B knockdown resulted in the increase in AMPK α 2 protein and in phospho-AMPK α 2, which is indicative of AMPK α 2 activation.

3.3. Knockdown of ARID5B mRNA extended the half-life of AMPK α 2 protein

In order to understand the mechanisms by which ARID5B knockdown increases AMPK α 2 levels, we first compared AMPK α 2 mRNA levels in cells transfected with siRNA or control scramble RNA. The results showed no difference (data not shown), which suggested that ARID5B is not involved in transcriptional regulation of AMPK α 2. Next, we investigated the stability of AMPK α 2 protein. Cells transfected with siRNA or control scramble RNA (Figure 3A) were subjected to treatment with cycloheximide (CHX) or MG132, and their effects on inhibition of AMPK α 2 protein synthesis or proteasomal degradation were measured. A representative result from two CHX experiments is shown in Figures 3B and 3C. In the absence of CHX, the level of AMPK α 2 protein was elevated by ARID5B knockdown HL-1 cells by more than 2-fold (compare Figure 3B lanes 1 and 5). In the presence of CHX the level of AMPK α 2 protein declined rapidly at 30 min, then recovered slowly over the next 2 h in the control cells (Figure 3B lanes 1-4). In contrast, the levels of AMPK α 2 protein remained elevated in ARID5B knockdown cells for 1 h, even when compared to the levels of AMPK α 2 protein in control cells in the absence of CHX (compare Figure 3B lanes 1 to lanes 6 and 7). These results suggest that AMPK α 2 protein appears more stable when ARID5B mRNA level is reduced.

When cells were treated with 10 μ M MG132, a slight increase in AMPK α 2 protein was seen in the control cells after 4 and 8 h-incubation (Figures 3D and 3E). This indicated that AMPK α 2 protein is being accumulated in HL-1 cells due to the inhibition of proteasome-mediated protein degradation as expected. In siRNA-transfected cells, a significant elevation of

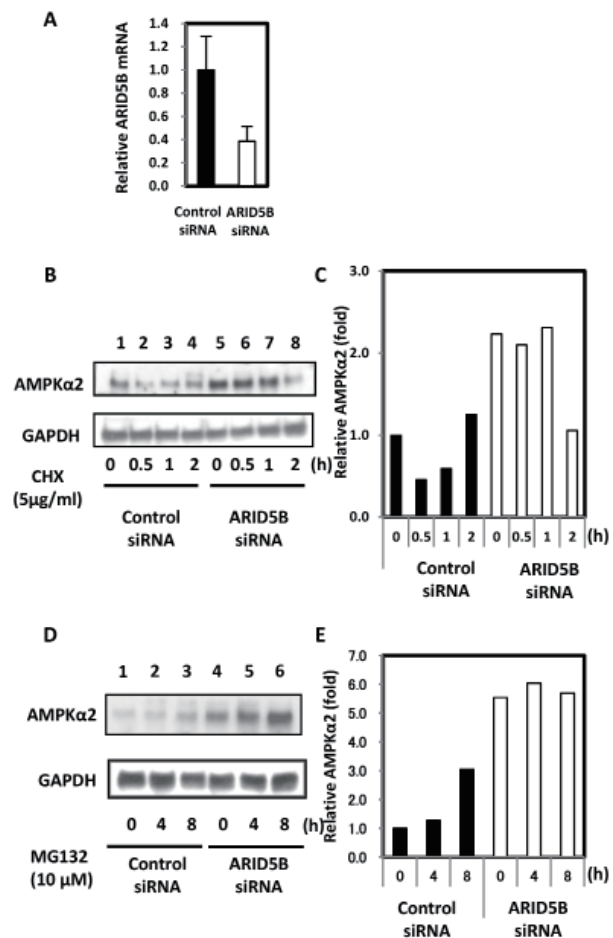


Figure 3. Knockdown of ARID5B increases the half-life of AMPK α 2 protein. A representative result of two independent experiments is shown. **A:** HL-1 cells were seeded in 35 mm dishes. siRNA efficiency was confirmed by qPCR at 48 h post-transfection. **B:** At 48 h post-transfection, HL-1 cells were treated with cycloheximide (CHX) (5 μ g/mL) for 0, 0.5, 1, or 2 h to block protein synthesis. Cell lysates were prepared and 20 μ g protein per lane was immunoblotted with anti-AMPK α 2 antibody. GAPDH was used as a loading control. **C:** Quantification of AMPK α 2 bands as shown in **B**. **D:** At 48 h post-transfection, HL-1 cells were treated with 10 μ M MG132 for 0, 4, or 8 h. Then cell lysates were prepared and 20 μ g protein per lane was immunoblotted with anti-AMPK α 2 antibody. GAPDH was used as a loading control. **E:** Quantification of AMPK α 2 as shown in **D**. In **A**, **C**, and **E**, shown are results from control (■) and ARID5B siRNA experiments (□).

AMPK α 2 protein (an average of 4-fold at 0 h) was observed, again confirming the results described in section 3.2. The effect of MG132 was also seen in an accumulation of AMPK α 2 protein after 4 or 8 h-incubation but to a lesser extent (Figures 3D and 3E), which may indicate that the AMPK α 2 protein expression had already saturated at 0 h of MG132 treatment in cells when ARID5B mRNA was knocked down.

The results shown in Figure 3 thus suggested that knockdown of ARID5B mRNA most likely extended the half-life of AMPK α 2 protein. It remains to be answered how ARID5B controls the stability of AMPK α 2 protein.

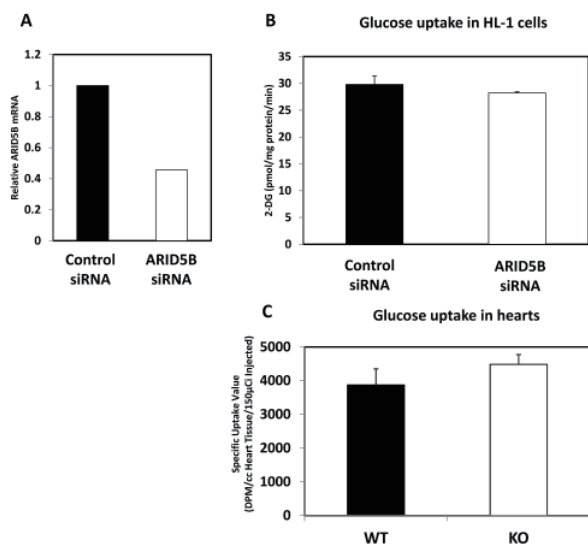


Figure 4. Glucose uptake in ARID5B knockdown HL-1 cells and in the hearts of wild-type and ARID5B knockout mice. **A:** HL-1 cells were seeded in 24-well plates. siRNA efficiency was confirmed by qPCR at 48 h post-transfection. RNA was isolated from three wells of a 24-well plate and the combined samples were analyzed for mRNA expression levels as described in Methods. **B:** At 48 h post-transfection, the cells were washed with KRPH buffer, and incubated with 2-deoxy-D- ^3H glucose for 10 min. Then cells were lysed with 0.5 M NaOH and radioactivity in the cell lysate was measured by scintillation counting. Results were calculated as pmol of glucose uptake per min per mg of protein ($n = 3$ per each group). In **A** and **B**, shown are results from control (■) and ARID5B siRNA experiments (□). **C:** PET imaging of heart tissue in *ARID5B*^{-/-} and *ARID5B*^{+/+} male mice. Three mice each of genotype were injected with ^{18}F -fluorodeoxyglucose and imaged after a 1 h uptake period. PET images of each heart were analyzed, and the specific uptake values were calculated as described in Methods. Shown are results from wild-type (WT) control (■) and ARID5B knockout (KO) experiments (□).

3.4. Glucose uptake in ARID5B knockdown HL-1 cells and hearts of ARID5B knockout mice

Next, we investigated possible physiological consequences of high levels of activated AMPK α 2 protein which is considered to be a sensor and regulator of energy balance at the cellular level. Since AMPK α 2 activation clearly occurs in the ARID5B knockdown cells, glucose uptake, one of possible physiological change, was measured in cells transfected with siRNA and control scramble RNA. The results, which are summarized in Figures 4A and 4B, did not show any significant differences in glucose uptake in those cells, however. Glucose uptake in HL-1 cardiomyocytes did respond to the AMPK mimetic AICAR which we used for control experiments. When added at 0.5 mM to the media 1 h prior to glucose uptake experiments, AICAR stimulated glucose uptake in non-treated and scramble RNA-treated cells increased 1.2 ± 0.13 ($n = 3$, $p > 0.05$) and 1.3 ± 0.03 ($n = 3$, $p < 0.01$)-fold, respectively. These effects, though small, positively demonstrated the correlation of glucose uptake and AMPK activation in HL-1 cells.

In order to investigate whether a decrease in

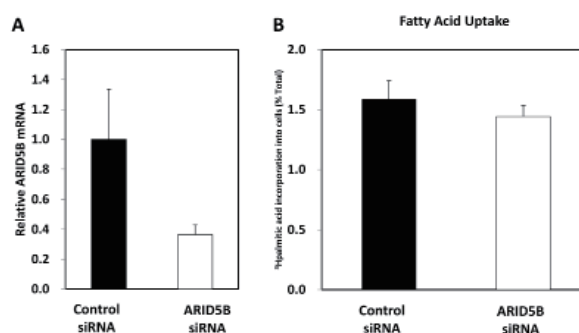


Figure 5. Fatty acid uptake in control and ARID5B knockdown HL-1 cells. **A:** HL-1 cells were seeded in 24-well plates. siRNA efficiency was confirmed by qPCR at 48 h post-transfection. **B:** HL-1 cells were seeded in 24-well plates and at 48 h post-transfection HL-1 cells were incubated for 15 min at 37°C in KRPH buffer, then incubated with ^3H palmitic acid for 20 min. Incubation medium was collected and the cells were lysed with 0.5 M NaOH. ^3H in the incubated medium and cell lysate was measured by scintillation counting. ^3H palmitic acid incorporation into cells was calculated as described in Methods and is shown as percentage of total ($n = 6$ for control; $n = 10$ for ARID5B siRNA). Shown are results from control (■) and ARID5B siRNA experiments (□).

ARID5B expression affects glucose uptake in live animals, positron emission tomography (PET) for glucose uptake in the hearts of wild-type and *ARID5B* knockout mice ($n = 3$) was performed. Although some tendency of a slight increase was observed in glucose uptake in the hearts of *ARID5B* knockout mice as compared to that in the hearts of wild type mice, the difference was not statically significant (Figure 4C).

3.5. Fatty acid uptake in ARID5B knockdown HL-1 cells

Generally speaking, the adult heart utilizes fatty acids as its main energy source (27). Thus, it can be speculated that fatty acid utilization may be affected by ARID5B knockdown. No difference in fatty acid uptake was, however, observed between control and ARID5B knockdown HL-1 cells (Figure 5).

4. Discussion

We demonstrated that siRNA efficiently knocked down *ARID5B* gene expression (to an average of 38% of control levels) in mouse cardiomyocyte HL-1 cells. AMPK α 2 protein levels were elevated in ARID5B knockdown HL-1 cells, and this was accompanied by an increase in the phosphorylation of AMPK α 2. Thus, in short, this study provided the foundation for an *in vitro* cell culture system to study possible roles of ARID5B in cardiomyocytes. This experimental *in vitro* cell culture may be useful in studying cardiac metabolism in pathophysiological conditions such as diabetic cardiomyopathy (28).

It has been well documented that activation of AMPK increases glucose uptake. Specifically, activation of AMPK *via* AICAR increased glucose uptake in

heart muscle (20) and in cardiac myocytes (21). Mice lacking AMPK α 2 or expressing dominant negative AMPK α 2 showed an inhibition of ischemia-induced stimulation of glucose uptake in cardiac muscle (22-24). In HL-1 cells it has been shown that insulin or the AMPK activator oligomycin stimulated glucose uptake by inducing translocation of GLUT4 (30). Adiponectin treatment also enhanced glucose and fatty acid uptake in HL-1 cells, and these effects were accompanied by increased AMPK phosphorylation (31). Based on previous reports, AMPK α 2 activation in ARID5B knockdown HL-1 cells would be expected to result in increase in glucose and/or fatty acid uptake. When the functional consequences of the AMPK α 2 activation induced by ARID5B knockdown in HL-1 cells were evaluated, however, under the culture conditions used in this study, we did not observe changes in glucose uptake (Figure 4), glycolysis (data not shown), fatty acid uptake (Figure 5), and fatty acid oxidation (data not shown). Further studies are obviously required to identify which metabolic pathways are affected by AMPK α 2 activation in HL-1 cells.

Since AMPK α 2 mRNA levels were not affected by ARID5B knockdown in HL-1 cells, the stability of AMPK α 2 protein was investigated using an inhibitor of protein synthesis (CHX) and an inhibitor of the proteasome degradation pathway (MG132). AMPK α 2 protein levels remained significantly elevated for an hour following CHX treatment in ARID5B knockdown HL-1 cells, while AMPK α 2 protein levels fell dramatically in control cells. These results indicated that ARID5B knockdown extends the half-life of AMPK α 2 protein in HL-1 cells. On the other hand, MG132 increased AMPK α 2 protein levels three-fold in control cells, but had no effect in ARID5B knockdown HL-1 cells. It should be noted that the level of AMPK α 2 protein in MG132-treated control cells was only half that of untreated ARID5B knockdown cells, even after eight hours of treatment. Wang *et al.* showed that calorie restriction (CR) increased the protein level of AMPK α 2 and phosphorylation of AMPK α 2 in skeletal muscle of wild-type mice, and that these changes in skeletal muscle contributed to an increase in whole body insulin sensitivity (32). CR did not increase insulin sensitivity in AMPK α 2^{-/-} mice. They also demonstrated that CR serum increased the stability of AMPK α 2 protein in C2C12 myoblasts by inhibiting ubiquitination of AMPK α 2 (32). Another study showed that life-long CR elicits a myocardial phenotype that is profoundly protected against ischemia/reperfusion injury, and that AMPK activation may play an important role in this process (33). It has been suggested that ubiquitination of AMPK in the heart may play a significant role in the etiology of cardiac diseases, and that this process presents an attractive target for developing novel therapies (34). In this regard, our finding that ARID5B may de-stabilize AMPK α 2 protein in cardiomyocytes is intriguing. Whether or not

the regulation of AMPK by ubiquitination is involved in this phenomenon requires further investigation.

In summary, this study provided the foundation for an *in vitro* cell culture system to study possible roles of ARID5B in cardiomyocytes. Further studies are required to understand the link between ARID5B knockdown and resulting AMPK α 2 activation and the possible involvement of the ubiquitin proteasome system in AMPK α 2 activation.

Acknowledgements

We thank Drs. W. Claycomb and M. Lam of LSU Health Science Center for providing us with HL-1 cells and very helpful instructions on culture conditions. The author (L H.-Y.) also thanks members of Dr. Itakura's laboratory for their continuous support and encouragement, and for Drs. M. Matsumoto and M. Kasuga at Research Institute National Center for Global Health and Medicine for their support.

References

- Huang TH, Oka T, Asai T, Okada T, Merrills BW, Gertson PN, Whitson RH, Itakura K. Repression by a differentiation-specific factor of the human cytomegalovirus enhancer. *Nucleic Acids Res.* 1996; 24:1695-1701.
- Yuan YC, Whitson RH, Liu Q, Itakura K, Chen Y. A novel DNA-binding motif shares structural homology to DNA replication and repair nucleases and polymerases. *Nature Structural Biology.* 1998; 5:959-964.
- Zhu L, Hu J, Lin D, Whitson R, Itakura K, Chen Y. Dynamics of the Mrf-2 DNA-binding domain free and in complex with DNA. *Biochemistry.* 2001; 40:9142-9150.
- Whitson RH, Huang T, Itakura K. The novel Mrf-2 DNA-binding domain recognizes a five-base core sequence through major and minor-groove contacts. *Biochem Biophys Res Commun.* 1999; 258:326-331.
- Kortschak RD, Tucker PW, Saint R. ARID proteins come in from the desert. *Trends Biochem Sci.* 2000; 25:294-299.
- Wilsker D, Patsialou A, Dallas PB, Moran E. ARID proteins: A diverse family of DNA binding proteins implicated in the control of cell growth, differentiation, and development. *Cell Growth Differ.* 2002; 13:95-106.
- Patsialou A, Wilsker D, Moran E. DNA-binding properties of ARID family proteins. *NucleicAcids Res.* 2005; 33:66-80.
- Lin C, Song W, Bi X, Zhao J, Huang Z, Li Z, Zhou J, Cai J, Zhao H. Recent advances in the ARID family: Focusing on roles in human cancer. *Onco Targets Ther.* 2014; 7:315-324.
- Watanabe M, Layne MD, Hsieh CM, Maemura K, Gray S, Lee ME, Jain MK. Regulation of smooth muscle cell differentiation by AT-rich interaction domain transcription factors Mrf2alpha and Mrf2beta. *Circ Res.* 2002; 91:382-389.
- Lahoud MH, Ristevski S, Venter DJ, Jermini LS, Bertoncello I, Zavarsek S, Hasthorpe S, Drago J, de Kretser D, Hertzog PJ, Kola I. Gene targeting of Desrt, a

- novel ARID class DNA-binding protein, causes growth retardation and abnormal development of reproductive organs. *Genome Res.* 2001; 8:1327-1334.
11. Wang G, Watanabe M, Imai Y, Hara K, Manabe I, Maemura K, Horikoshi M, Kohro T, Amiya E, Sugiyama T, Fujita T, Kadowaki T, Yamazaki T, Nagai R. Genetic variations of Mrf-2/ARID5B confer risk of coronary atherosclerosis in the Japanese population. *Int Heart J.* 2008; 49:313-327.
 12. Wang G, Watanabe M, Imai Y, Hara K, Manabe I, Maemura K, Horikoshi M, Ozeki A, Itoh C, Sugiyama T, Kadowaki T, Yamazaki T, Nagai R. Associations of variations in the MRF2/ARID5B gene with susceptibility to type 2 diabetes in the Japanese population. *J Hum Genet.* 2012; 57:727-733.
 13. Whitson RH, Tsark W, Huang TH, Itakura K. Neonatal mortality and leanness in mice lacking the ARID transcription factor Mrf-2. *Biochem Biophys Res Commun.* 2003; 312:997-1004.
 14. Yamakawa T, Whitson RH, Li SL, Itakura K. Modulator recognition factor-2 is required for adipogenesis in mouse embryo fibroblasts and 3T3-L1 cells. *Mol Endocrinol.* 2008; 22:441-453.
 15. Steinberg GR, Kemp BE. AMPK in Health and Disease. *Physiol Rev.* 2009; 89:1025-1078.
 16. Carling D. The AMP-activated protein kinase cascade – A unifying system for energy control. *Trends Biochem Sci.* 2004; 29:18-24.
 17. Kahn BB, Alquier T, Carling D, Hardie DG. AMP-activated protein kinase: Ancient energy gauge provides clues to modern understanding of metabolism. *Cell Metab.* 2005; 1:15-25.
 18. Merrill GF, Kurth EJ, Hardie DG, Winder WW. AICA riboside increases AMP-activated protein kinase, fatty acid oxidation, and glucose uptake in rat muscle. *Am J Physiol.* 1997; 273:E1107-12.
 19. Zhou G, Myers R, Li Y, Chen Y, Shen X, Fenyk-Melody J, Wu M, Ventre J, Doeber T, Fujii N, Musi N, Hirshman MF, Goodyear LJ, Moller DE. Role of AMP-activated protein kinase in mechanism of metformin action. *J Clin Invest.* 2001; 108(8):1167-74.
 20. Russell RR 3rd, Bergeron R, Shulman GI, Young LH. Translocation of myocardial GLUT-4 and increased glucose uptake through activation of AMPK by AICAR. *Am J Physiol.* 1999; 277:H643-649.
 21. Horie T, Ono K, Nagao K, Nishi H, Kinoshita M, Kawamura T, Wada H, Shimatsu A, Kita T, Hasegawa K. Oxidative stress induces GLUT4 translocation by activation of PI3-K/Akt and dual AMPK kinase in cardiac myocytes. *J Cell Physiol.* 2008; 215:733-742.
 22. Carvajal K, Zarrinpashneh E, Szarszoi O, Joubert F, Athes Y, Mateo P, Gillet B, Vaulont S, Viollet B, Bigard X, Bertrand L, Ventura-Clapier R, Hoerter JA. Dual cardiac contractile effects of the alpha2-AMPK deletion in low-flow ischemia and reperfusion. *Am J Physiol Heart Circ Physiol.* 2007; 292:H3136-H3147.
 23. Russell RR 3rd, Li J, Coven DL, Pypaert M, Zechner C, Palmeri M, Giordano FJ, Mu J, Birnbaum MJ, Young LH. AMP-activated protein kinase mediates ischemic glucose uptake and prevents postischemic cardiac dysfunction, apoptosis, and injury. *J Clin Invest.* 2004; 114:495-503.
 24. Xing Y, Musi N, Fujii N, Zou L, Luptak I, Hirshman MF, Goodyear LJ, Tian R. Glucose metabolism and energy homeostasis in mouse hearts overexpressing dominant negative alpha2 subunit of AMP-activated protein kinase. *J Biol Chem.* 2003; 278:28372-28377.
 25. Claycomb WC, Lanson NA Jr, Stallworth BS, Egeland DB, Delcarpio JB, Bahinski A, Izzo NJ Jr. HL-1 cells: A cardiac muscle cell line that contracts and retains phenotypic characteristics of the adult cardiomyocyte. *Proc Natl. Acad. Sci. U S A.* 1998; 95:2979-2984.
 26. White SM, Constantin PE, Claycomb WC. Cardiac physiology at the cellular level: Use of cultured HL-1 cardiomyocytes for studies of cardiac muscle cell structure and function. *Am J Physiol Heart Circ Physiol.* 2004; 286:H823-829.
 27. Kodde IF, van der Stok J, Smolenski RT, de Jong JW. Metabolic and genetic regulation of cardiac energy substrate preference. *Comparative Biochemistry and Physiology Part A: Molecular & Integrative Physiology.* 2007; 146:26-39.
 28. An D, Rodrigues B. Role of changes in cardiac metabolism in development of diabetic cardiomyopathy. *Am J Physiol Heart Circ Physiol.* 2006; 291:H1489-506.
 29. Palanivel R, Eguchi M, Shuralyova I, Coe I, Sweeney Gary. Distinct effects of short- and long-term leptin treatment on glucose and fatty acid uptake and metabolism in HL-1 cardiomyocytes. *Metabolism and Clinical Experimental.* 2006; 55:1067-1075.
 30. Schwenk RW, Dirx E, Coumans WA, Bonen A, Klip A, Glatz JF, Luiken JJ. Requirement for distinct vesicle-associated membrane proteins in insulin- and AMP-activated protein kinase (AMPK)-induced translocation of GLUT4 and CD36 in cultured cardiomyocytes. *Diabetologia.* 2010; 53:2209-2219.
 31. Piñeiro R, Iglesias MJ, Gallego R, Raghay K, Eiras S, Rubio J, Diéguez C, Gualillo O, González-Juanatey JR, Lago F. Adiponectin is synthesized and secreted by human and murine cardiomyocytes. *FEBS Lett.* 2005; 579:5163-5169.
 32. Wang P, Zhang RY, Song J, Guan YF, Xu TY, Du H, Viollet B, Miao CY. Loss of AMP-activated protein kinase- α 2 impairs the insulin-sensitizing effect of calorie restriction in skeletal muscle. *Diabetes.* 2012; 61:1051-1061.
 33. Edwards AG, Donato AJ, Lesniewski LA, Gioscia RA, Seals DR, Moore RL. Life-long caloric restriction elicits pronounced protection of the aged myocardium: A role for AMPK. *Mech Ageing Dev.* 2010; 131:739-742.
 34. Zungu M, Schisler JC, Essop MF, McCudden C, Patterson C, Willis MS. Regulation of AMPK by the ubiquitin proteasome system. *Am J Pathol.* 2011; 178:4-11.

(Received November 20, 2015; Revised December 20, 2015; Accepted December 20, 2015)